Am J Transl Res 2025;17(12):9531-9541
www.ajtr.org /ISSN:1943-8141/AJTR0167435

Original Article

Analysis of bioglass/cerium dioxide nanocoating and its antibacterial properties for the restoration of hard tissue around oral titanium implants

Rui Chen[1], Yudong Jia[2], Xiaoxu Ren[3], Gang Guo[3]

[1]Department of Stomatology, Shanxi Bethune Hospital, Shanxi Academy of Medical Sciences, Tongji Shanxi Hospital, Third Hospital of Shanxi Medical University, Tongji Hospital, Tongji Medical College, Huazhong University of Science and Technology, Taiyuan 030032, Shanxi, China; [2]Dental Medicine, Shanxi Medical University, Taiyuan 030000, Shanxi, China; [3]Department of Stomatology, Changzhi People's Hospital of Shanxi Province, Changzhi 046000, Shanxi, China

Received July 14, 2025; Accepted November 27, 2025; Epub December 15, 2025; Published December 30, 2025

Abstract: Objective: To investigate peri-implant hard tissue regeneration by developing a novel titanium (Ti) implant coated with a composite nanocoating of bioglass (BG) and cerium dioxide (CeO_2). Methods: The BG/CeO_2 composite coating was fabricated on Ti implants using liquid-feed flame spray pyrolysis. The coating's morphology and composition were characterized by scanning electron microscopy and X-ray diffraction. Its antibacterial efficacy was assessed against *Porphyromonas gingivalis* (*P. gingivalis*). The cytocompatibility, osteogenic differentiation, and mineralization potential were evaluated using human dental pulp stem cells (DPSCs). Additionally, rabbit mandibular defect models were established to investigate the anti-inflammatory, antioxidant, and osteogenic properties of the implants *in vivo*. Results: The CeO_2 nanocoatings exhibited significant antibacterial activity against *P. gingivalis* while demonstrating excellent biocompatibility and a marked stimulation of DPSC proliferation. The CeO_2/BG-Ti implants were more effective in enhancing DPSC activity and upregulating the expression of osteogenesis-related proteins than control groups. In rabbit models, the CeO_2/BG-Ti implants effectively mitigated oxidative stress and reduced the secretion of inflammatory factors, thereby alleviating the post-operative inflammatory response. Furthermore, improved bone healing and enhanced new bone formation were observed around the CeO_2/BG-Ti implants, leading to superior implant stability and osseointegration. Conclusions: The CeO_2/BG-Ti composite implants demonstrate considerable potential for clinical use in oral implantology, offering enhanced antibacterial, anti-inflammatory, and osteogenic benefits.

Keywords: Bioglass, cerium dioxide, titanium implants, nanoparticles, osseointegration, antibacterial, oral cavity

Introduction

Titanium (Ti) implants have revolutionized dentistry due to their favorable biocompatibility and mechanical properties, with widespread applications including single-tooth replacements, full-arch prosthetic support, and orthodontic anchorage [1-6]. These implants effectively restore masticatory function, phonetics, and aesthetics, significantly improving patients' quality of life. However, implant failure remains a concern, often resulting from poor osseointegration, peri-implantitis, biomechanical overloading, or insufficient bone volume [7, 8]. Such complications may lead to implant loosening or loss, necessitating additional surgical intervention, and increasing patient burden [9, 10]. Therefore, enhancing the long-term stability and biological performance of Ti implants is critically important.

Recent advances in nanotechnology have led to the development of various nanocoatings to improve implant osseointegration. Among them, bioglass (BG) is a biomaterial commonly used for the repair of bone defects, offering several benefits and advancements in the field of implant dentistry [11]. Relevant studies have found that BG has the unique property of bonding with bone tissue when it comes into contact with bodily fluids, promoting faster and stronger osseointegration between the implant and the

surrounding bone [12]. Moreover, it can promote the formation of new bone tissue in the implant site, which is particularly beneficial in cases with insufficient bone volume or compromised bone quality [13]. Nevertheless, it's important to note that bacterial colonization and infection around the implant site is a key cause leading to implant failure, such as peri-implantitis. Thus, further optimization of BG composition is needed to incorporate effective antibacterial function.

Cerium dioxide (CeO_2) nanoparticles (NPs) have recently emerged as a promising bioactive agent for implant modification due to their beneficial effects. For example, Ceria NPs possess unique antioxidant properties, which can enhance the longevity and performance of Ti implants [14]. In addition, it has been found that Ceria NPs have demonstrated antibacterial properties against various bacterial strains commonly associated with implant-related infections, which can help prevent or minimize the risk of implant-associated infection [15]. Based on this rationale, we proposed that incorporating CeO_2 into a BG-based coating on Ti implants could synergistically enhance antibacterial capacity while supporting osseointegration.

At present, studies on the use of CeO_2 and BG in Ti implants are still in early stages, and more are needed to explain their potential benefits and long-term effects. This study aimed to investigate whether it is possible to create a favorable environment for osseointegration by modifying the implant surface with CeO_2 and BG, thereby reducing the risk of bacterial colonization and promoting better tissue integration.

Materials and methods

Preparation of CeO_2/BG-Ti implant

The CeO_2/BG hybrid NPs were fabricated and applied to Ti implants by a two-step process based on liquid-feed flame spray pyrolysis (LF-FSP) [16]. First, in the synthesis step, a precursor solution - comprising 68 wt% cerium(III) nitrate, 11 wt% calcium acetylacetonate hydrate, 13 wt% sodium 2-ethylhexanoate, 2 wt% tributyl phosphate, and 6 wt% hexamethyldisiloxane in tetrahydrofuran (THF) (yielding a final CeO_2 to BG mass ratio of ~1:0.5) - was fed at 5 mL/min into a water-cooled nozzle, dispersed by O_2 (5 L/min), and ignited by a CH_4/O_2 flame. Ti disks were placed 6 cm above the flame for 25 s to directly deposit the CeO_2/BG NPs. Then, during the deposition step, collected NPs were first collected on a filter, dispersed in a mixture of water, acetylacetone, and Triton X-100, and then was spin-coated onto the Ti implant surface using a spin-coater (VTC-100, Kejing Automation Equipment Co., Ltd., Shenyang, China) at 1000 rpm for 60 s. Pure CeO_2 and BG control coatings were prepared separately using analogous methods, with the following precursor compositions: CeO_2: 100 wt% cerium(III) 2-ethylhexanoate in THF. BG: 40 wt% calcium acetylacetonate hydrate, 37 wt% sodium 2-ethylhexanoate, 6 wt% tributyl phosphate, 17 wt% hexamethyldisiloxane in THF (**Figure 1**).

Cell culture

Human dental pulp stem cells (DPSCs, CP-H231) were selected to study the osteogenic properties of CeO_2 *in vitro*. DPSCs were cultured in a 24-well plate with their special medium (CM-H231) in a cell incubator for 24 h. The cultured DPSCs were diluted to 1×10^6/ml for standby. The cells and cell culture media used were purchased from Wuhan Procell Life Technology Co., Ltd.

Preparation of CeO_2 suspensions

The CeO_2 NPs were dissolved in 0.9% NaCl solution and subsequently sonicated for 2 min at 0°C to prepare the CeO_2 suspension, and the CeO_2 suspension was diluted to 25%, 50% and 100% concentrations.

Detection of physicochemical properties of CeO_2/BG-Ti

The appearance of CeO_2 NPs: The shape and size of the CeO_2 NPs were examined by scanning electron microscope (SEM, Sigma, Jena, Germany).

X-ray diffractometer of CeO_2/BG-Ti: To observe the composition of the surface coating of Ti implants, X-ray diffractometer (XRD, POWDIX 600/300, Beijing Oubeier Scientific Instrument Co., Ltd.) was used to check its characterization.

CeO_2 antibacterial property testing: Porphyromonas gingivalis (*P. gingivalis*, ATCCBAA-3083, Shanghai Conservation Biotechnology Center,

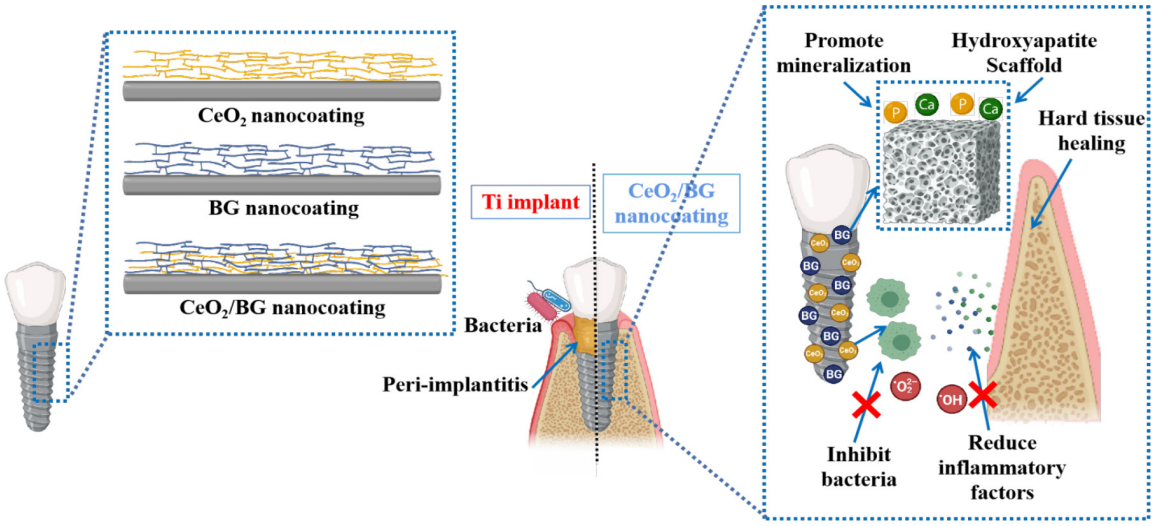

Figure 1. Mechanism of CeO_2/BG Ti implants for peri-implant hard tissue recovery. CeO_2: Cerium dioxide; BG: Bioglass; Ti: Titanium.

Table 1. PCR primer information

	F primer	R primer
RUNX2	5'-TTCAACGATCTGAGATTTGTGGG-3'	5'-GGATGAGGAATGCGCCCTA-3'
ALP	5'-AACCCAGACACAAGCATTCC-3'	5'-CCAGCAAGAAGAAGCCTTTG-3'
Col I	5'-CACCCTCAAGAGCCTGAGTC-3'	5'-CGGGCTGATGTACCAGTTCT-3'
β-actin	5'-CTGGCACCACACCTTCTACA-3'	5'-GGTACGACCAGAGGCATACA-3'

PCR: Polymerase chain reaction; RUNX2: Runt-related transcription factor 2; ALP: Alkaline phosphatase; Col I: Type I collagen.

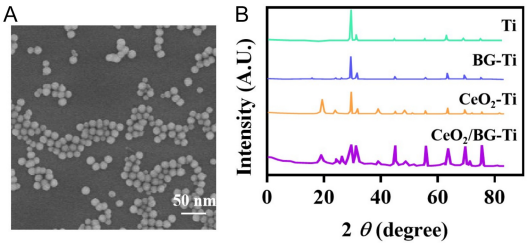

Figure 2. SEM of CeO_2 nanoparticles (A) and XRD of Ti implants with different coatings (B). Scale bar: 50 nm. SEM: Scanning electron microscope; CeO_2: Cerium dioxide; BG: Bioglass; Ti: Titanium; XRD: X-ray diffractometer.

China) was selected for antibacterial test. *P. gingivalis* was cultured in Columbia blood tablet (CA-B) (BHY-2132, Shanghai Boohoo Biotechnology Co., Ltd., China) under 37°C, 80%N_2, 10% CO_2, and 10% H_2 for 72 h. The colonies were then diluted to a concentration of 1 × 10^6 CFU/mL by serial dilution and prepared for use. 1 ml of *P. gingivalis* suspension was cultured in Columbia blood tablet, and divided into control (without any intervention) and CeO_2 groups (treated with 25%, 50%, and 100% CeO_2 suspensions). Activation state of *P. gingivalis* was tested by live/dead bacterial kit (04511, Sigma, USA), and the surviving bacteria are stained with green fluorescence and observed with a fluorescent microscope colored green and fluoresced and observed with a confocal microscope (SP8, Leica, Wetzlar, Germany).

Meanwhile, intracellular reactive oxygen species (ROS) levels in *P. gingivalis* were detected using the fluorescent probe DCFH-DA (Beyotime Biotechnology, China).

CeO_2 biocompatibility testing: 1 ml of DPSCs dilution was inoculated on 12-well plates and divided into control (without any intervention) and CeO_2 groups (treated with 25%, 50% and 100% CeO_2 suspensions), with 3 replicate wells in each group. 24 h after incubation, Anti-filamentous actin antibody [NH3] (ab205) was added to label the viable cytoskeleton and fluorescein isothiocyanate (FITC, ab6717) was added as a fluorescent secondary antibody,

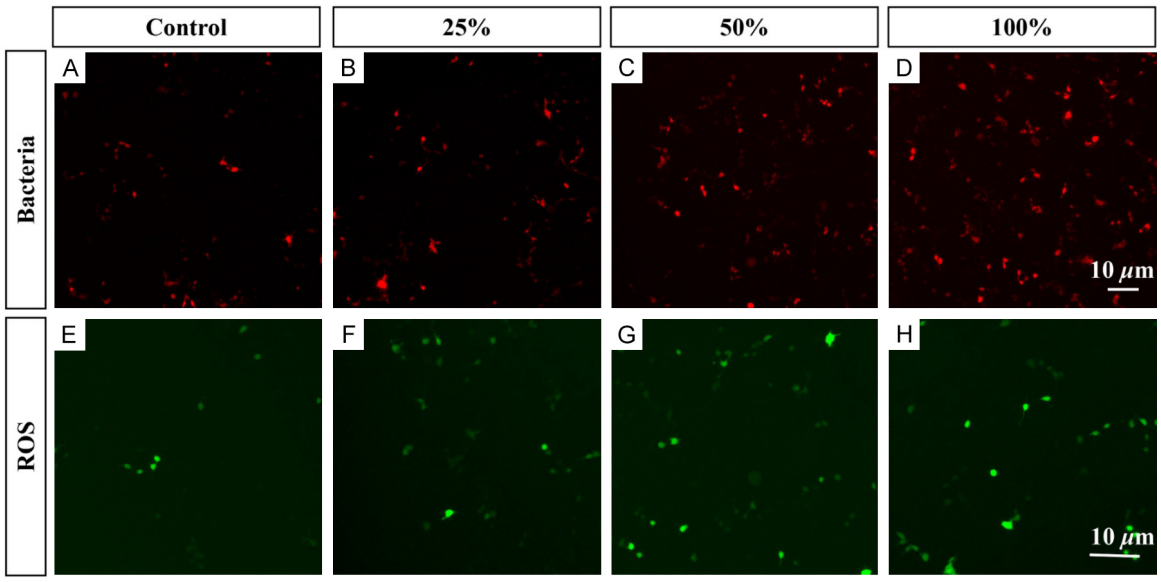

Figure 3. Detection of CeO_2 nanoparticles' antibacterial activity. A-D: Fluorescent staining of dead *P. gingivalis* in the control and CeO_2 groups with different concentrations, 10×. E-H: Fluorescent staining of ROS in the control and CeO_2 groups with different concentrations, 10×. Scale bar: 10 μm. CeO_2: Cerium dioxide; ROS: Reactive oxygen species.

while 4', 6-diamidino-2-phenylindole dihydrochloride (DAPI, ab285390) was used to stain the nuclei of the viable cells. Finally, the fluorescent staining of the cells in each group was observed using a confocal microscope. All reagents were purchased from Abcam, Waltham, MA, USA.

DPSCs activity assay

1 ml of DPSCs dilution was inoculated in a 12-well plate with its special culture medium and divided into Ti (treated with Ti implant), BG-Ti (treated with BG-Ti implant), and CeO_2/BG-Ti groups (treated with CeO_2/BG-Ti implant) with 3 replicate wells. After incubation at 37°, 5% CO_2 for 24 h, fluorescent staining of the surviving cells in each group was examined using the same method described in section 2.4.4.

DPSCs mineralization function assay

1 ml of DPSCs dilution was inoculated in 12-well plate and divided into Ti [osteoinduction medium (HUXDP-90021, Saiye Biotechnology Co., Ltd., Suzhou, China) + Ti implant], BG-Ti (osteoinduction medium + BG-Ti implant), and CeO_2/BG-Ti groups (osteoinduction medium + CeO_2/BG-Ti implant) with three replicate wells in each group. After 7 days of incubation, the levels of runt-related transcription factor 2 (RUNX2), alkaline phosphatase (ALP), and type I collagen (Col I) were measured in each group. Briefly, Anti-RUNX2 (ab192256), Anti-ALP (ab224335), and Anti-Col I (ab34710) were used to label the above osteogenic proteins in cells, and FITC, ALP (ab6722), and Alexa Fluor® 405 (ab175652) were added as fluorescent secondary antibodies. Finally, the fluorescent staining was observed in each group using confocal microscopy. Meanwhile, relative expression of the above indexes in each group was quantitatively detected by polymerase chain reaction (PCR) (**Table 1**). All reagents used were purchased from Abcam.

Implant placement surgery

36 New Zealand white rabbits weighted 4.5-5 kg were chosen for animal tests. The rabbits were randomly divided into Ti, BG-Ti, and CeO_2/BG-Ti groups, with 12 rabbits in each group. After general anesthesia with 3% pentobarbital sodium, the rabbits were gingivally separated and their two mandibular anterior teeth were extracted, followed by insertion of Ti, BG-Ti, and CeO_2/BG-Ti implants into their sockets, and final suturing of the gingiva to cover the implants. Post-operative intramuscular penicillin sodium was administered for 3 consecutive days to combat infection and the maxillary anterior teeth were polished weekly to avoid damage to the wound.

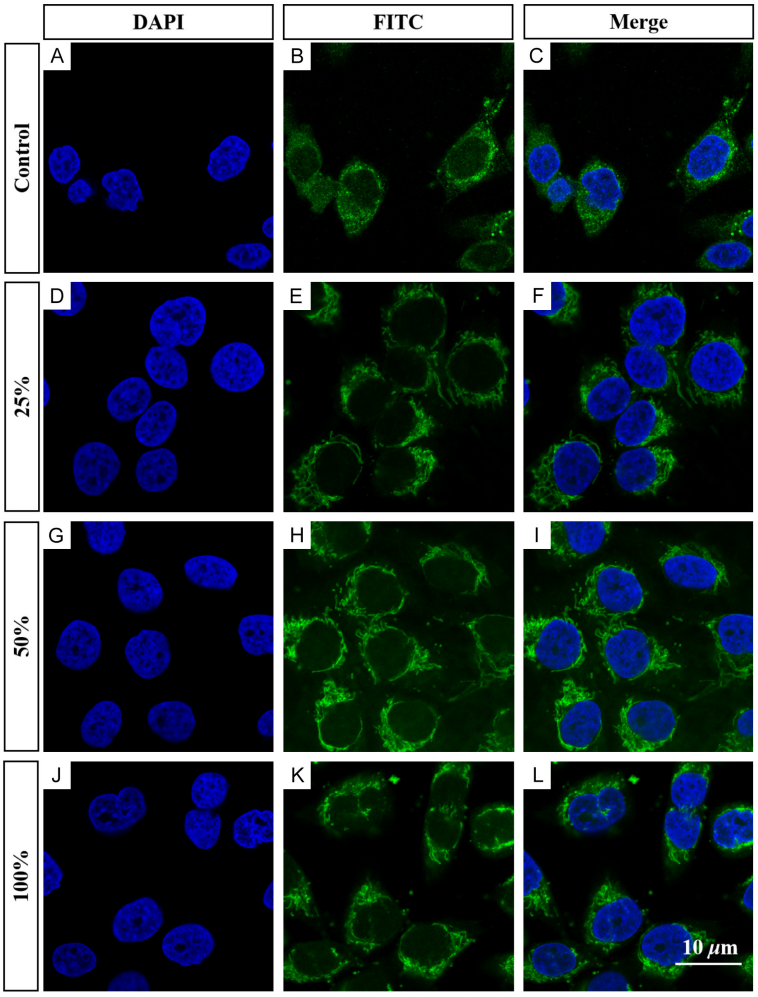

Figure 4. Fluorescent staining of DPSC nuclei, F-actin, and both combined in the control (A-C) and 25% (D-F), 50% (G-I), and 100% (J-L) CeO_2 groups, 40×. Scale bar: 10 μm. DPSC: Dental pulp stem cell; FITC: Fluorescein isothiocyanate; DAPI: 4',6-diamidino-2-phenylindole dihydrochloride; CeO_2: Cerium dioxide.

Detection of inflammatory response

At 3 weeks post-operation, three randomly selected rabbits from each group were euthanized, and their mandibles were dissected. Bone blocks containing the implants were meticulously sectioned. After careful removal of the implants, all surrounding soft and hard tissues within the sockets were harvested using a sterile curette. The acquired tissue specimens were thoroughly homogenized and centrifuged to obtain the supernatant for subsequent analysis. Levels of IL-1β (ab197742), IL-6 (ab222503), and TNF-α (ab208348) were then measured by ELISA. All kits were purchased from Abcam.

Detection of oxidative stress

As described in section 2.8, the acquired tissue specimens were thoroughly homogenized and centrifuged to obtain the supernatant. The levels of superoxide dismutase (SOD), malondialdehyde (MDA), and total antioxidant capacity (TAC) were then measured by ELISA. The corresponding kits were purchased from Nanjing Jiancheng BioEngineering Institute.

Peri-implant osteogenesis test

New Zealand rabbits in each group were randomly divided into 1-, 2-, and 3- month groups and sacrificed at 1, 2, and 3 months postoperatively to obtain peri-implant mandibular bone specimens respectively. Twenty-seven mandibular bone samples were then scanned using micro-CT (SKYSCAN 1276, BRUKER, Karlsruhe, Germany) and the accompanying Java software was used to calculate the bone volume fraction (BV/TV), trabecular thickness (Tb.Th), and total porosity [Po(tot)] of the interest area 1 mm from the implant to quantitatively assess the healing of the peri-implant bone tissue. During the measurement, the irregularities in the image were manually selected to exclude the cortical bone in the interest area and to retain only the trabecular for evaluation.

Statistical analysis

All data were analyzed using GraphPad Prism 7 (GraphPad Software, USA) and are presented as mean ± standard deviation (SD). Differences between two groups were assessed using the two-tailed Student's t-test, while one-way analysis of variance (ANOVA) followed by Tukey's post hoc test was used for multiple group comparisons. Statistical significance was set at $*P* < 0.05$.

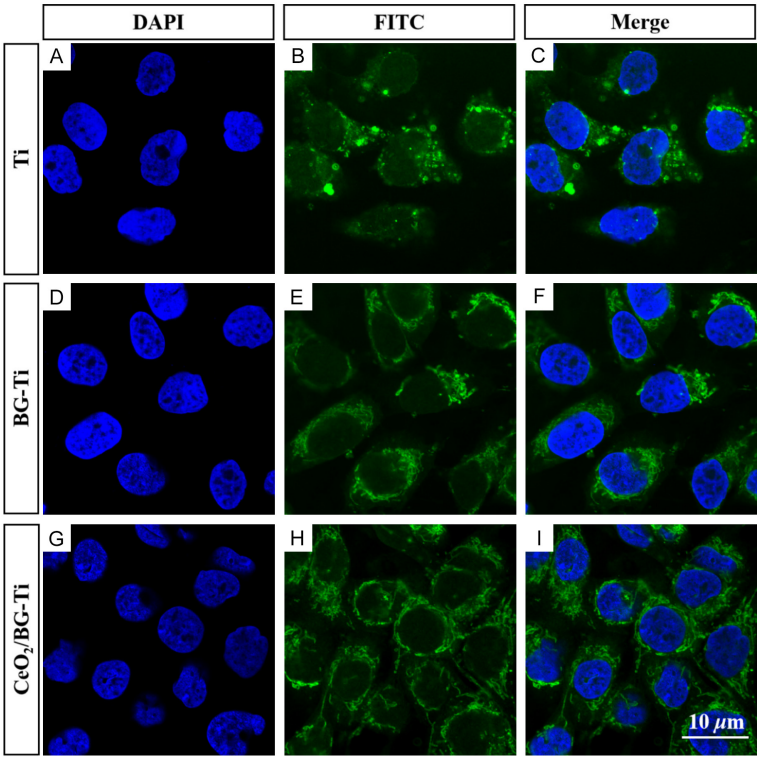

Figure 5. Fluorescent staining of DPSC nuclei, F-actin, and both combined in the Ti (A-C), BG-Ti (D-F), and CeO_2/BG-Ti (G-I) groups, 40×. Scale bar: 10 μm. DPSC: Dental pulp stem cell; FITC: Fluorescein isothiocyanate; DAPI: 4',6-diamidino-2-phenylindole dihydrochloride; CeO_2: Cerium dioxide; BG: Bioglass; Ti: Titanium.

Results

Physicochemical property testing

The average particle size of CeO_2 NPs was approximately 10-20 nm (**Figure 2A**). To investigate the composition of the Ti implant surface coating, the characterization of the coating was analyzed by XRD. The results showed that the CeO_2, BG, and CeO_2/BG coatings all had a clear Ti background, with the BG coating only appearing as a visible small angular diffraction peak, indicating that most of the BG did not remain in the crystalline state. In contrast, the CeO_2 and CeO_2/BG coatings showed several characteristic diffraction peaks, suggesting that CeO_2 formed a crystalline phase in the coating (**Figure 2B**).

CeO_2 could effectively inhibit P. gingivalis proliferation

The staining of surviving *P. gingivalis* was observed by fluorescence microscopy, and it was found that CeO_2 could effectively inhibit the activity of *P. gingivalis* and inhibit their proliferation, and its inhibitory property was further enhanced with increasing concentration (**Figure 3A-D**). As the concentration of the CeO_2 suspension increased, the intracellular ROS level in bacteria rose correspondingly (**Figure 3E-H**). Thus, CeO_2 has marked antibacterial properties and is concentration-dependent.

CeO_2 showed good biocompatibility

Fluorescence microscopic observation showed that the addition of CeO_2 effectively enhanced the activity of DPSCs compared to those cultured alone, and their number further increased with increasing concentration of CeO_2 suspensions (**Figure 4**). Thus, CeO_2 is biocompatible and can effectively enhance DPSC activity in a concentration-dependent manner.

CeO_2/BG-Ti could better enhance DPSCs activity

Under fluorescence microscopy, cell adhesion was observed on the surface of Ti implants covered with different coatings. More DPSCs were observed on the surface of BG- and CeO_2/BG-Ti implants compared to Ti implants alone, especially in the CeO_2/BG-Ti group (**Figure 5**). Therefore, CeO_2/BG-Ti can more effectively promote DPSC proliferation.

CeO_2/BG-Ti could better enhance the mineralization of DPSCs

To assess the osteoinductive function of CeO_2/BG, we examined the expression of relevant osteogenic proteins in DPSCs. We found that the expression levels of RUNX 2, ALP, and COL I were markedly increased in the BG- and CeO_2/BG-Ti groups compared to DPSCs cultured with Ti implants, especially in the CeO_2/BG-Ti group (**Figure 6A-I**). The quantitative PCR analysis of the above indicators in each group also demonstrated the same results (**Figure 6J**). Thus,

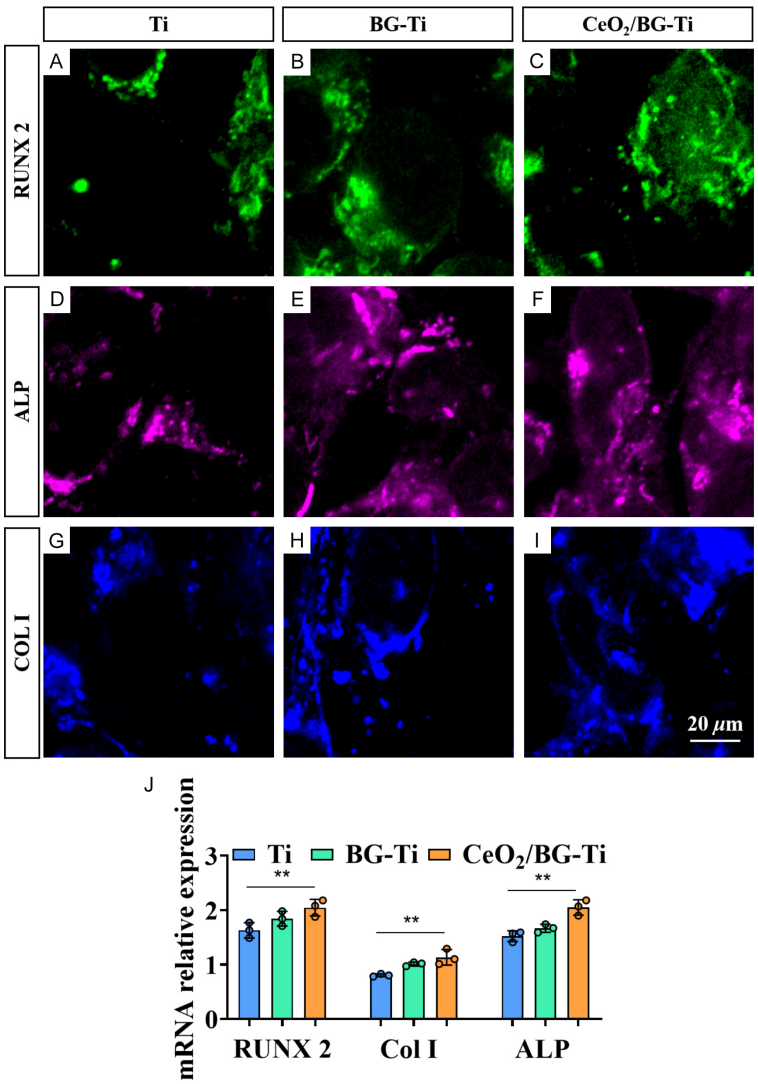

Figure 6. Detection of DPSC mineralization. A-C: RUNX2 fluorescent staining in DPSCs cultured with Ti, BG-Ti, or CeO_2/BG-Ti implants, 40×. D-F: ALP fluorescent staining in DPSCs cultured with Ti, BG-Ti, or CeO_2/BG-Ti implants, 40×. G-I: COL I fluorescent staining in DPSCs cultured with Ti, BG-Ti, or CeO_2/BG-Ti implants, 40×. J: The quantitative PCR analysis of RUNX2, ALP, and COL I. Scale bar: 20 μm. $^{**}P < 0.01$. n=3. DPSC: Dental pulp stem cell; RUNX2: Runt-related transcription factor 2; ALP: Alkaline phosphatase; Col I: Type I collagen; CeO_2: Cerium dioxide; BG: Bioglass; Ti: Titanium; PCR: Polymerase chain reaction.

CeO_2/BG-Ti could better enhance the mineralization function of DPSCs and promote bone tissue repair.

CeO_2/BG-Ti implants effectively inhibited the inflammatory response

After implantation of different Ti implants, the levels of IL-1β, IL-6, and TNF-α were higher in rabbits in the Ti and BG/Ti groups than in the CeO_2/BG-Ti group (**Figure 7**). Therefore, the CeO_2/BG coating could better suppress the inflammatory response after implant placement.

CeO_2/BG-Ti implants could effectively inhibit oxidative stress

Oxidative stress levels provide a useful assessment of the occurrence of inflammatory responses *in vivo*. SOD and TAC levels in rabbits were markedly lower in the Ti and BG/Ti groups than in the CeO_2/BG-Ti group, in contrast to the significant increase in MDA levels that occurred (**Figure 8**). Thus, the CeO_2/BG coating is effective in suppressing the degree of oxidative stress after implant insertion.

CeO_2/BG-Ti can best promote peri-implant hard tissue recovery

By observing the peri-implant bone tissue by micro-CT, we found that BV/TV and Tb.Th were markedly higher in the area 1 mm from the BG- and CeO_2/BG-Ti implants compared to the Ti implants, and that these indicators continued to increase with time of implantation, especially in the CeO_2/BG-Ti group (**Figure 9A-D**). In contrast, Po(tot) was markedly lower in the BG- and CeO_2/BG-Ti groups than in the Ti group and continued to decrease with increasing implantation time, especially in the CeO_2/BG-Ti group (**Figure 9E**, **9F**). CeO_2/BG-Ti therefore better promotes the regeneration and maturation of the bone tissue around the implant for its better stability.

Discussion

In this study, we developed a novel CeO_2/BG composite coating for titanium implants to enhance osseointegration - the direct structur-

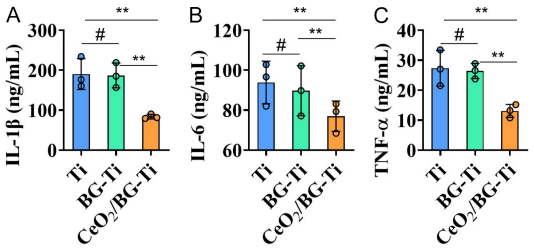

Figure 7. Comparison of IL-1β (A), IL-6 (B), and TNF-α (C) levels in rabbit models treated with Ti, BG/Ti, and CeO_2/BG-Ti implants. #P > 0.05, **P < 0.01. n=3. CeO_2: Cerium dioxide; BG: Bioglass; Ti: Titanium.

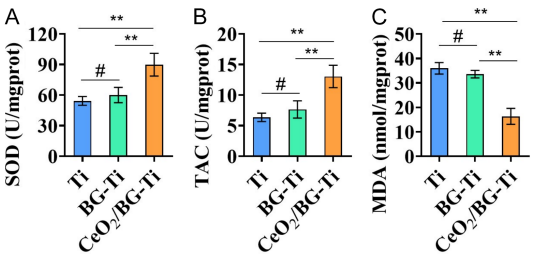

Figure 8. Comparison of SOD (A), TAC (B), and MDA (C) levels in rabbit models treated with Ti, BG/Ti, and CeO_2/BG-Ti implants. #P > 0.05, **P < 0.01. n=3. SOD: Superoxide dismutase; TAC: Total antioxidant capacity; MDA: Malondialdehyde; CeO_2: Cerium dioxide; BG: Bioglass; Ti: Titanium; Prot: Protein.

al and functional connection between living bone and the implant surface. Our findings demonstrate that this coating exhibits excellent antibacterial properties, promotes stem cell proliferation and osteogenic differentiation, and reduces inflammatory and oxidative stress *in vivo*, collectively contributing to improved bone regeneration and implant stability.

Physicochemical characterization confirmed the successful synthesis of CeO_2 nanoparticles with a size of approximately 10-20 nm and the formation of a crystalline CeO_2 phase within the composite coating. The antibacterial assays revealed that CeO_2 effectively inhibited the growth of *P. gingivalis* in a concentration-dependent manner. Li et al. [17] also found that CeO_2 could effectively inhibit the proliferation of various bacteria and had good antibacterial properties. The potent antibacterial activity observed in our study can be primarily attributed to the ROS generation mediated by CeO_2 NPs. Our experimental data provide direct evidence that intracellular ROS levels in *P. gingivalis* increased significantly in a dose-dependent manner with the concentration of CeO_2 NPs. This is consistent with the established ability of CeO_2 NPs to cycle between Ce^{3+} and Ce^{4+} oxidation states, catalyzing the production of superoxide and hydroxyl radicals [18]. These highly reactive species can inflict severe damage to essential bacterial components, including DNA, proteins, and lipids. Furthermore, we speculate that the observed antibacterial effect is likely exacerbated by the potential of CeO_2 NPs to interfere with bacterial antioxidant defense systems, such as catalase and superoxide dismutase, thereby hindering the clearance of ROS and promoting its accumulation [19]. The elevated oxidative stress is expected to induce lipid peroxidation, which directly compromises the integrity of the bacterial cell membrane. While direct visual evidence from techniques such as transmission electron microscopy (TEM) for membrane disruption is beyond the scope of this study, the measured ROS surge strongly implies that membrane damage is a probable consequential event leading to increased permeability and eventual cell death [20]. In addition to its antibacterial role, CeO_2 showed significant biocompatibility and even a stimulatory effect on DPSC proliferation. This finding is supported by Ren et al. [21], who found that periodontal ligament stem cells cultured with CeO_2 NPs exhibited increased cell proliferation compared to cells cultured alone, possibly by enhancing cellular metabolic activity. Therefore, the above findings indicate the potential of CeO_2 coating for inhibiting peri-implantitis and promoting DPSC proliferation.

The CeO_2/BG-Ti implants markedly enhanced DPSC proliferation and osteogenic differentiation compared to Ti or BG-Ti controls. The reason maybe that the BG component can promote DPSCs adhesion [22], release osteogenic ions such as calcium and phosphate, and mimic the mineral composition of natural bone, which facilitate DPSC mineralization [24, 25]. CeO_2 NPs exhibit anti-inflammatory properties, which can create a more favorable microenvironment for DPSCs proliferation [23]. Notably, it has been reported that the controlled production of ROS by CeO_2 NPs can act as signaling molecules to stimulate osteogenic differentiation in other stem cell types [26]. We hypothesize that a ROS-mediated pathway contributes to the upregulation of osteogenic markers (e.g., RUNX2, ALP, COL I) and enhanced mineralization observed in our experiments - a phe-

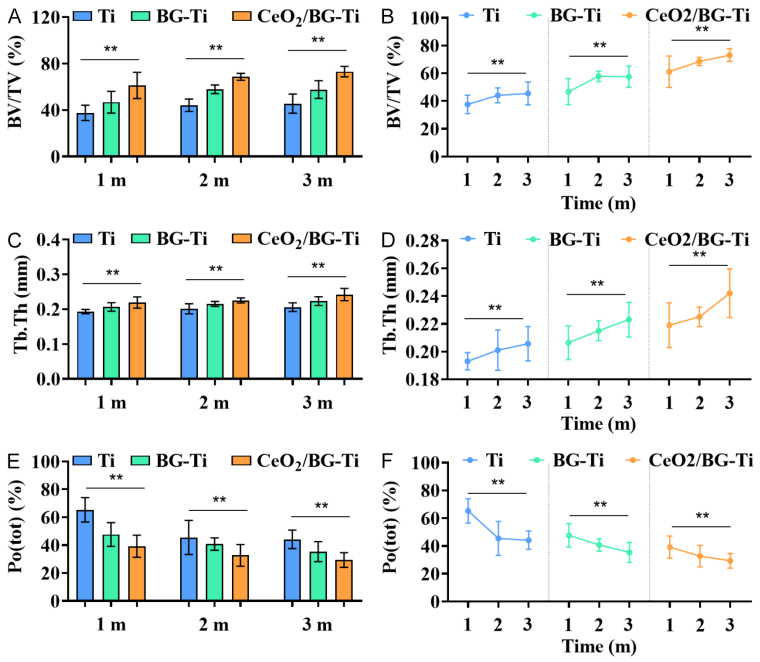

Figure 9. Comparison of peri-implant hard tissue recovery in terms of BV/TV (A, B), Tb.Th (C, D), and Po(tot) (E, F) in rabbit models treated with Ti, BG/Ti, and CeO_2/BG-Ti implants at 1, 2, and 3 months. $^{**}P < 0.01$. n=3. BV/TV: Bone volume fraction; Tb.Th: Trabecular thickness; Po(tot): Porosity; CeO_2: Cerium dioxide; BG: Bioglass; Ti: Titanium.

nomenon also reported in bone marrow stromal cells by Li et al. [27]. However, the precise signaling mechanism requires further validation through ROS-scavenging or gene-knockdown approaches.

The *in vivo* results further confirmed the beneficial effects of the CeO_2/BG coating. Implants coated with CeO_2/BG exhibited the most markedly suppressed oxidative stress and inflammatory response. This suggests that CeO_2 exerts antioxidant effects under physiologic conditions, likely due to its pH-dependent catalytic activity. In the physiologic pH of the healing peri-implant tissue, CeO_2 acts as a potent antioxidant, scavenging excess ROS and thereby mitigating oxidative damage and subsequent inflammation. This role is crucial for creating a favorable microenvironment for bone regeneration [28]. Moreover, micro-CT consistently demonstrated superior bone healing and osseointegration around the CeO_2/BG-Ti implants. The reason may be that BG has the ability to form a hydroxyapatite layer on its surface when in contact with bodily fluids, which mimics the mineral composition of natural bone, making it highly compatible with the surrounding bone [29, 30].

Thus, the incorporated CeO_2 plays a crucial dual role: it not only helps prevent bacterial colonization - a significant risk factor for peri-implantitis and implant failure [31] - but also, as previously discussed, mitigates local oxidative stress and inflammation Therefore, the combination of BG's osteoconductivity and CeO_2's antibacterial/antioxidant properties synergistically facilitate better bone healing and exerts a more pronounced osteogenic effect.

Despite these promising results, our study has several limitations. First, evidence for CeO_2-induced bacterial membrane damage remains indirect; future studies should include direct visualization via TEM. Second, we did not set up a separate CeO_2-Ti group in animal experiments to better investigate its anti-inflammatory and antioxidant effects. Finally, the mechanistic role of CeO_2 in promoting DPSC differentiation - particularly the involvement of ROS-related signaling pathways - was not directly verified through interventional experiments such as ROS scavenging or genetic knockdown. In a follow-up study, we need to further improve the above deficiencies to guide the later clinical trials.

Conclusion

CeO_2 NPs can effectively inhibit *P. gingivalis* proliferation and have good biocompatibility with DPSCs. The combination of BG and CeO_2 coating can more effectively promote the proliferation and mineralization of DPSCs, thus effectively improving the repair of peri-implant hard tissues. When CeO_2/BG composite implants are placed in animal models, they effectively inhibit the degree of oxidative stress and the release of inflammatory factors, and exert osteogenic properties, providing a good microenvironment for the healing of the hard tissue around the implant. This creation of a conducive microenvironment for peri-implant healing may improve the long-term success of dental implants.

Disclosure of conflict of interest

None.

Address correspondence to: Gang Guo, Department of Stomatology, Changzhi People's Hospital of Shanxi Province, Changzhi 046000, Shanxi, China. Tel: +86-0355-2066181; E-mail: 00000gogog@163.com

References

[1] Kheder W, Al Kawas S, Khalaf K and Samsudin AR. Impact of tribocorrosion and titanium particles release on dental implant complications - a narrative review. Jpn Dent Sci Rev 2021; 57: 182-189.

[2] Apaza-Bedoya K, Tarce M, Benfatti CAM, Henriques B, Mathew MT, Teughels W and Souza JCM. Synergistic interactions between corrosion and wear at titanium-based dental implant connections: a scoping review. J Periodontal Res 2017; 52: 946-954.

[3] Pesce P, Menini M, Santori G, Giovanni E, Bagnasco F and Canullo L. Photo and plasma activation of dental implant titanium surfaces. a systematic review with meta-analysis of preclinical studies. J Clin Med 2020; 9: 2817.

[4] Liu X, Chen S, Tsoi JKH and Matinlinna JP. Binary titanium alloys as dental implant materials-a review. Regen Biomater 2017; 4: 315-323.

[5] Cervino G, Fiorillo L, Iannello G, Santonocito D, Risitano G and Cicciu M. Sandblasted and acid etched titanium dental implant surfaces systematic review and confocal microscopy evaluation. Materials (Basel) 2019; 12: 1763.

[6] Al-Meraikhi H, Yilmaz B, McGlumphy E, Brantley WA and Johnston WM. Distortion of CAD-CAM-fabricated implant-fixed titanium and zirconia complete dental prosthesis frameworks. J Prosthet Dent 2018; 119: 116-123.

[7] Paparella ML, Domingo MG, Puia SA, Jacobi-Gresser E and Olmedo DG. Titanium dental implant-related pathologies: a retrospective histopathological study. Oral Dis 2022; 28: 503-512.

[8] Yu YJ, Zhu WQ, Xu LN, Ming PP, Shao SY and Qiu J. Osseointegration of titanium dental implant under fluoride exposure in rabbits: Micro-CT and histomorphometry study. Clin Oral Implants Res 2019; 30: 1038-1048.

[9] Annunziata M and Guida L. The effect of titanium surface modifications on dental implant osseointegration. Front Oral Biol 2015; 17: 62-77.

[10] Safi IN, Hussein BMA, Al Shammari AM and Tawfiq TA. Implementation and characterization of coating pure titanium dental implant with sintered beta-TCP by using Nd: YAG laser. Saudi Dent J 2019; 31: 242-250.

[11] Riva F, Bloise N, Omes C, Ceccarelli G, Fassina L, Nappi RE and Visai L. Human ovarian follicular fluid mesenchymal stem cells express osteogenic markers when cultured on bioglass 58s-coated titanium scaffolds. Materials (Basel) 2023; 16: 3676.

[12] Jurczyk K, Adamek G, Kubicka MM, Jakubowicz J and Jurczyk M. Nanostructured titanium-10 wt% 45S5 bioglass-ag composite foams for medical applications. Materials (Basel) 2015; 8: 1398-1412.

[13] Mani N, Sola A, Trinchi A and Fox K. Is there a future for additive manufactured titanium bioglass composites in biomedical application? A perspective. Biointerphases 2020; 15: 068501.

[14] Rosario F, Costa C, Lopes CB, Estrada AC, Tavares DS, Pereira E, Teixeira JP and Reis AT. In vitro hepatotoxic and neurotoxic effects of titanium and cerium dioxide nanoparticles, arsenic and mercury co-exposure. Int J Mol Sci 2022; 23: 2737.

[15] Tumburu L, Andersen CP, Rygiewicz PT and Reichman JR. Molecular and physiological responses to titanium dioxide and cerium oxide nanoparticles in Arabidopsis. Environ Toxicol Chem 2017; 36: 71-82.

[16] Matter MT, Furer LA, Starsich FHL, Fortunato G, Pratsinis SE and Herrmann IK. Engineering the bioactivity of flame-made ceria and ceria/bioglass hybrid nanoparticles. ACS Appl Mater Interfaces 2019; 11: 2830-2839.

[17] Li X, Qi M, Sun X, Weir MD, Tay FR, Oates TW, Dong B, Zhou Y, Wang L and Xu HHK. Surface treatments on titanium implants via nanostructured ceria for antibacterial and anti-inflammatory capabilities. Acta Biomater 2019; 94: 627-643.

[18] Tumburu L, Andersen CP, Rygiewicz PT and Reichman JR. Phenotypic and genomic responses to titanium dioxide and cerium oxide nanoparticles in Arabidopsis germinants. Environ Toxicol Chem 2015; 34: 70-83.

[19] He P, Zhao Z, Tan Y, E H, Zuo M, Wang J, Yang J, Cui S and Yang X. Photocatalytic degradation of deoxynivalenol using cerium doped titanium dioxide under ultraviolet light irradiation. Toxins (Basel) 2021; 13: 481.

[20] Ma Y, Metch JW, Vejerano EP, Miller IJ, Leon EC, Marr LC, Vikesland PJ and Pruden A. Microbial community response of nitrifying sequencing batch reactors to silver, zero-valent iron, titanium dioxide and cerium dioxide nanomaterials. Water Res 2015; 68: 87-97.

[21] Ren S, Zhou Y, Zheng K, Xu X, Yang J, Wang X, Miao L, Wei H and Xu Y. Cerium oxide nanoparticles loaded nanofibrous membranes promote

bone regeneration for periodontal tissue engineering. Bioact Mater 2022; 7: 242-253.
[22] Anindyajati A, Boughton P and Ruys AJ. Mechanical and cytocompatibility evaluation of UHMWPE/PCL/bioglass((R)) fibrous composite for acetabular labrum implant. Materials (Basel) 2019; 12: 916.
[23] Andersen CP, King G, Plocher M, Storm M, Pokhrel LR, Johnson MG and Rygiewicz PT. Germination and early plant development of ten plant species exposed to titanium dioxide and cerium oxide nanoparticles. Environ Toxicol Chem 2016; 35: 2223-2229.
[24] Ma X, Schou KR, Maloney-Schou M, Harwin FM and Ng JD. The porous polyethylene/bioglass spherical orbital implant: a retrospective study of 170 cases. Ophthalmic Plast Reconstr Surg 2011; 27: 21-27.
[25] Popa AC, Stan GE, Husanu MA, Mercioniu I, Santos LF, Fernandes HR and Ferreira J. Bioglass implant-coating interactions in synthetic physiological fluids with varying degrees of biomimicry. Int J Nanomedicine 2017; 12: 683-707.
[26] El Yamani N, Collins AR, Runden-Pran E, Fjellsbo LM, Shaposhnikov S, Zienolddiny S and Dusinska M. In vitro genotoxicity testing of four reference metal nanomaterials, titanium dioxide, zinc oxide, cerium oxide and silver: towards reliable hazard assessment. Mutagenesis 2017; 32: 117-126.
[27] Li K, Shen Q, Xie Y, You M, Huang L and Zheng X. Incorporation of cerium oxide into hydroxyapatite coating regulates osteogenic activity of mesenchymal stem cell and macrophage polarization. J Biomater Appl 2017; 31: 1062-1076.
[28] Yin M, Lei D, Liu Y, Qin T, Gao H, Lv W, Liu Q, Qin L, Jin W, Chen Y, Liang H, Wang B, Gao M, Zhang J and Lu J. NIR triggered polydopamine coated cerium dioxide nanozyme for ameliorating acute lung injury via enhanced ROS scavenging. J Nanobiotechnology 2024; 22: 321.
[29] Ananth KP, Suganya S, Mangalaraj D, Ferreira JM and Balamurugan A. Electrophoretic bilayer deposition of zirconia and reinforced bioglass system on Ti6Al4V for implant applications: an in vitro investigation. Mater Sci Eng C Mater Biol Appl 2013; 33: 4160-4166.
[30] Sultan S, Thomas N, Varghese M, Dalvi Y, Joy S, Hall S and Mathew AP. The design of 3D-printed polylactic acid-bioglass composite scaffold: a potential implant material for bone tissue engineering. Molecules 2022; 27: 7214.
[31] Liu X, Li Y, Zhou X, Luo K, Hu L, Liu K and Bai L. Photocatalytic degradation of dimethoate in Bok choy using cerium-doped nano titanium dioxide. PLoS One 2018; 13: e0197560.